Turkish Journal of Electrical Engineering & Computer Sciences

http://journals.tubitak.gov.tr/elektrik/

Research Article

Turk J Elec Eng & Comp Sci
(2020) 28: 93 – 106

doi:10.3906/elk-1902-81

Retinal vessel segmentation using modified symmetrical local threshold

Umar ÖZGÜNALP*
Department of Electrical and Electronics Engineering, Faculty of Engineering,
Cyprus International University, Nicosia, North Cyprus, Mersin, Turkey

Received: 11.02.2019 • **Accepted/Published Online:** 18.10.2019 • **Final Version:** 27.01.2020

Abstract: Retinal vessel segmentation is important for the identification of many diseases including glaucoma, hypertensive retinopathy, diabetes, and hypertension. Moreover, retinal vessel diameter is associated with cardiovascular mortality. Accurate detection of blood vessels improves the detection of exudates in color fundus images, as well as detection of the retinal nerve, optic disc, or fovea. A retinal vessel is a darker stripe on a lighter background. Thus, the objective is very similar to the lane detection task for intelligent vehicles. A lane on a road is a light stripe on a darker background (i.e. asphalt). For lane detection, the symmetrical local threshold (SLT) is found to be the most robust feature extractor among the tested algorithms in the road marking (ROMA) dataset. Unfortunately, the SLT cannot be applied directly for retinal vessel segmentation. The SLT is a 1D filter and is designed for detecting vertical or close to vertical light stripes with predictable width. In this paper, the SLT is modified to detect dark stripes and four kernels, instead of one, are designed to detect both vertical and horizontal features of a retinal vessel with variable thickness. The proposed algorithm is tested using the High Resolution Fundus (HRF) image database and the accuracy is estimated to be 95.53%. Furthermore, when tested with the Digital Retinal Images for Vessel Segmentation (DRIVE) database, the accuracy is estimated to be 93.69%.

Key words: Retinal vessel segmentation, feature extraction, symmetrical local threshold, retinopathy

1. Introduction

Ocular fundus images can reveal many pathological diseases related to the cardiovascular, endocrine-metabolic, and central-nervous systems [1]. Examination of the retinal vessel structure is also an important part of the diagnosis. For instance, tortuosity (nonsmooth course of the vessel) is associated with blood pressure and cardiovascular risks [2]. An association between retinal vessel diameter and cardiovascular mortality was found [2]. Furthermore, it is stated [3] that detection of blood vessels can improve the detection of exudates in a color fundus image. While detecting vascular trees can reveal useful information for the diagnosis of various diseases such as hypertension, diabetes, and glaucoma [4], an accurate detection result can also be used for locating the optic disc [5]. For the stated reasons, automatic detection of blood vessels from ocular fundus images is a vital task.

In the literature, many algorithms have been proposed based on both feature extraction and machine learning. Retinal vessel segmentation algorithms can be categorized into five groups [6]: pattern recognition based, matched filtering based, vessel tracking/tracing based, mathematical morphology based, model based,

*Correspondence: uozgunalp@ciu.edu.tr

and machine learning based. A Gaussian filter has been used to detect retinal vessels [7]. A matched filter is used as a feature extractor and vessels are detected using a high threshold [8]. Subsequently, additional vein pieces are added to the segmentation based on the initially detected starting points. A ridge detector is used to detect retinal vessels [9]. An improvement on the matched filter for retinal vessel segmentation has been proposed by measuring numerous perpendicular cross-sectional intensity profiles of retinal vessels and by designing the matched filter accordingly [4]. A genetic algorithm has been used to optimize the matched filter to detect retinal vessels [10]. Line tracking has been used to detect retinal vessels [11]. CNN-based vessel segmentation is described [12, 13] and retinal vessels are segmented using an extreme learning machine [14]. Veins are segmented based on creating a vein probability map by filtering images with second derivatives of Gaussians with multiple scales and calculating eigenvalues of the outputs [15]. A previously proposed algorithm first detects and in-paints exudates, then enhances vessels using multiscale Hessian eigenvalue analysis, and finally detects veins using percentile-based thresholding [16].

A discriminative dictionary learning-based retinal vessel segmentation algorithm is proposed, where the proposed algorithm uses fusion of multiple features [17]. Another study [18] utilizes active contours to segment out vessels. Palomera-Perez et al. [19] extracted multiscale features based on calculated Hessian values and enhanced the results by using a region growing algorithm. Zhang et al. [20] utilized a matched filter to detect retinal vessels. In the algorithm, while retinal vessels are detected by matched filter, the threshold is adjusted based on the first order derivative of Gaussian. The method proposed by Marin et al. [21] first extracts feature maps for vessel pixels and then employs a neural network to segment out vessel pixels.

In the present paper, a novel and accurate retinal vessel segmentation algorithm is proposed. The proposed algorithm is inspired by symmetrical local thresholding (SLT), which was originally proposed for lane detection (for intelligent vehicles). The detection of a lane from a road image and the detection of a vein from a retinal fundus image have certain similarities. For instance, detecting a lane marking requires the detection of a light stripe on a darker background and, in the case of veins, it is necessary to detect a darker stripe on a lighter background. In the literature, it can be seen that some of the generic computer vision algorithms are already common for both lane marking segmentation and retinal vessel segmentation. For instance, in Schreiber et al. [22], edge detection has been used to extract lane features and in Wand and Lee [23], edge detection has been used for vein segmentation. In Broggi et al. [24], a matched filter has been used to segment out lane markings and in Odstrcilik et al. [4], a matched filter has been used to segment out veins in retinal images. McCall and Trivedi [25, 26] used Gaussian filter-based lane feature extraction and Gang et al. [7] used a Gaussian filter for vein segmentation. Ridges have been used to extract lane features [27] and for vein segmentation [9]. Although there are many lane feature extractors in the literature, Veit et al. [28] tested the most common lane feature extractors and concluded that, despite its simplicity, the SLT algorithm is the most accurate among those tested. However, there are differences between veins and lanes. The thickness of a vein can change considerably compared to a lane marking. Furthermore, while lane markings are vertical or close to vertical, a vein can be in any orientation. SLT is specifically designed for lane marking extraction and thus several modifications are necessary to it for vein detection. Hence, in the present paper, a modified version of the SLT algorithm is proposed for vein segmentation on retinal images. The rest of the paper is organized as follows: in Section 2.1, the features of a vein on a digital fundus image are described. In Section 2.2, the standard SLT algorithm is described. In Section 2.3, proposed modifications to the SLT algorithm are described. In Section 2.4, the postprocessing applied is described. In Section 3, the experimental results are given and a comparison

is made in terms of sensitivity (SE), specificity (SP), and accuracy (ACC). Finally, in Section 4, the paper is concluded. The block diagram of the proposed algorithm is shown in Figure 1.

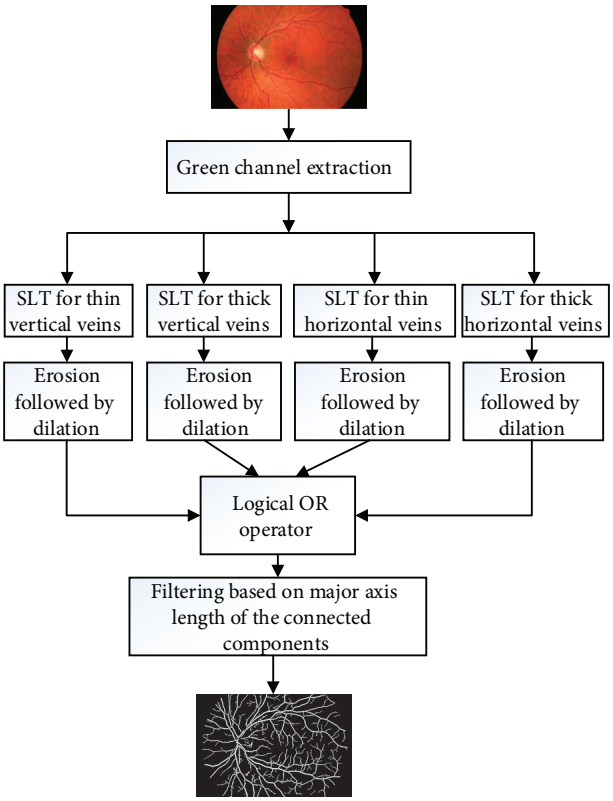

(a)

Figure 1: Block diagram of the proposed retinal vessel segmentation algorithm.

2. Materials and methods

2.1. Features of a vein on a digital fundus image

Conventionally, to segment retinal vessels, only the green channel of the image is used for vessel segmentation [4]. Thus, in the present paper, only the green channel of the RGB image is extracted (only the green pixel values are used and red and blue pixel values are ignored) and treated as a gray scale image. An example input fundus image and its single channel output is provided in Figure 2.

It is observed that a retinal vessel has a light–dark–light (LDL) property. This means that each pixel on a vein should have a lower intensity value compared to the two sides of the vessel. For instance, if the vein is vertical or close to vertical, the pixels on the left-hand side and the pixels on the right-hand side should both have higher intensity values. On the other hand, if the vein is horizontal, the pixels on the top and the pixels on the bottom should both have higher intensity values. This is demonstrated in Figure 3. In Figure 3a, an example of a vertical vein extracted from an ocular fundus image is demonstrated. In Figure 3b, an example of a horizontal vein extracted from an ocular fundus image is demonstrated. Another important property of a vein captured by an ocular fundus image is its thickness. The thickness of a vein can change considerably. This is demonstrated in Figure 4. In Figure 4a, an example image with thin veins is shown, while in Figure 4b, an example image with thick veins is shown. Both images are extracted from the same ocular fundus image. The

(a) (b)

Figure 2: An example RGB image captured by a fundus camera and its green channel.

algorithm proposed in the present paper is inspired by the SLT algorithm, which is useful for extracting lane markings from a road image. In the next section, the SLT algorithm and its use for lane marking extraction will be described. Then the properties of a lane and a vein will be compared and modifications to the SLT algorithm will be proposed for vein detection.

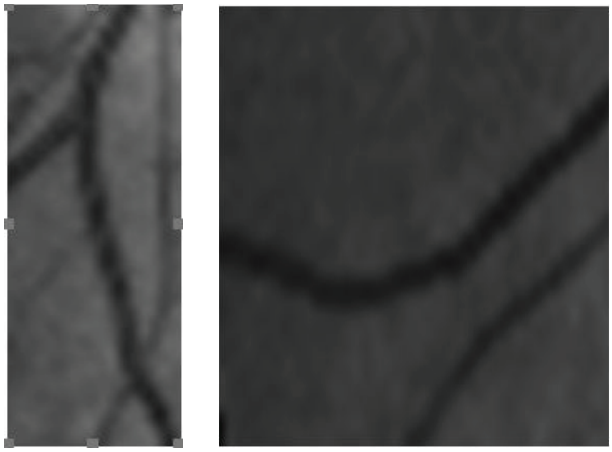

(a) (b)

Figure 3: Example cross-sectional areas for vertical and horizontal veins: (a) an example vertical vein extracted from an ocular fundus image, (b) an example horizontal vein extracted from an ocular fundus image.

2.2. Symmetrical local threshold

A lane departure warning system (LDWS) is a crucial component of intelligent vehicles. These systems are designed to warn the driver when the ego vehicle is departing from the road. The key component of a LDWS is lane detection. Lane detection algorithms can be divided into two categories: feature-based and model-based [29]. While feature-based lane detection algorithms segment lane markings or road area, model-based algorithms firstly extract the feature map and then based on certain assumptions such as fixed road curvature, fixed road width, or flat road, lanes are modeled (defined) by mathematical equations. In both cases, the first step is to segment the lane features. For lane feature extraction, many algorithms have been proposed including edge

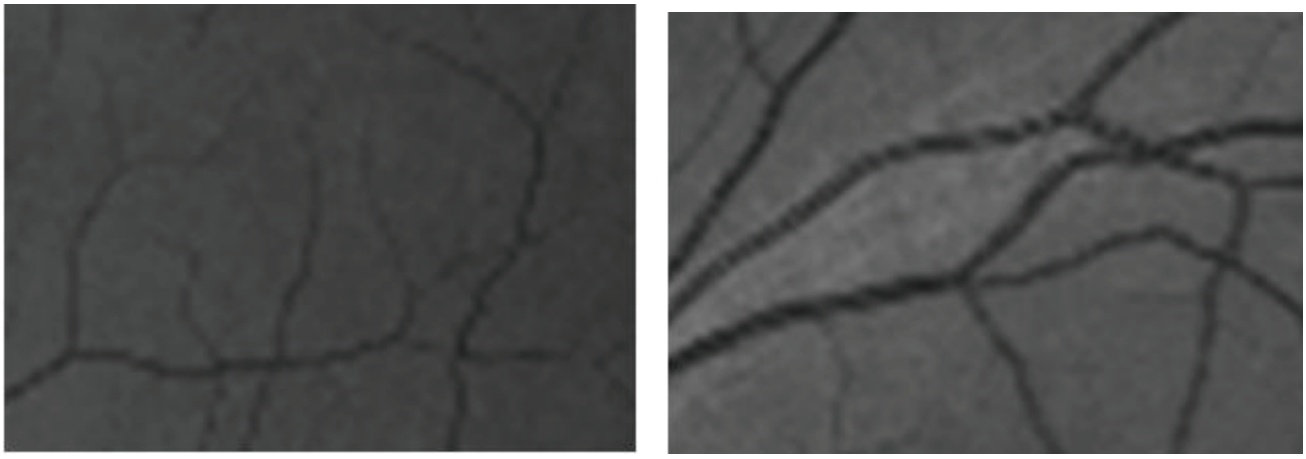

(a) (b)

Figure 4: Example cross-sectional areas for thin and thick veins: (a) an example thin vein, (b) an example thick vein, where there is a considerable thickness difference between two different veins in an ocular fundus image.

detectors [22], the Otsu algorithm [30], Gabor filters [31], local threshold [28], matched filters [24], and the SLT algorithm [32]. Although feature extraction is the first and most vital component of a lane detection system, there is no benchmark available for lane marking feature extraction. However, Veit et al. [28] implemented the most common lane feature extractors and compared them quantitatively using ground truths supplied in a road marking (ROMA) dataset. The ROMA dataset consists of 116 road images from diverse road scenes including variable lighting conditions, variable scene content, and variable road types. For these images, pixels from lane markings are manually labeled as ground truth lane pixels. Although the SLT algorithm offers simplicity, Veit et al. [28] concluded that it is the most robust feature extractor among those tested.

The SLT algorithm is designed to extract light stripes with vertical or near vertical slope. It processes images row by row independently. In each row of the image, for each pixel, it calculates the average of the pixels on the left-hand side within the range and then calculates the average of the pixels on the right-hand side within the range. If the intensity value of the pixel (Ip) minus a threshold (Th) value is larger than both left average ($Average_L$) and right average ($AverageR$), that pixel is estimated to be a feature point. As mentioned before, a lane marking has a dark–light–dark (DLD) property. DLD means that compared to the pixel intensity the pixels on the left and pixels on the right need to be darker. The threshold used (the threshold is set to be 4 for the experiments) is necessary to remove noise from homogeneous areas. The pseudocode of the algorithm is shown in Algorithm 1. The algorithm is illustrated in Figure 5, where the test pixel is shown with a blue dot and the area that is used to calculate the left average and the right average is shown with a yellow horizontal line.

2.3. Multiscale multidirectional SLT

There are several differences between lane markings and retinal vessels. First, retinal veins have a LDL property instead of DLD. Thus, pixel intensity plus a threshold needs to be lower than both the left average ($Average_L$) and right average ($Average_R$). For vein segmentation, the SLT algorithm is modified accordingly. Second, the SLT algorithm is a one-dimensional approach. Since a lane marking on a road image is assumed to be horizontal

Algorithm 1 Symmetrical local threshold

F $\leftarrow \emptyset$
while $I_p \in ImageSize$ **do**
  if $I_p - T_h > Average_R$ *and* $I_p - T_h > Average_L$ **then**
    $F_{Ip} \leftarrow 1$
  end if
end while

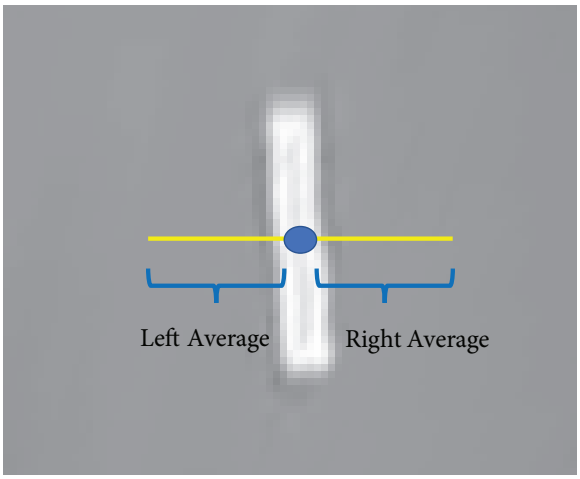

Figure 5: Illustration of the regions used for the SLT algorithm, where the test pixel is shown with a blue dot and the area that is used to calculate the left average and right average is shown with a yellow horizontal line.

or nearly horizontal, the DLD feature is checked from left to right. Veins can be both horizontal and vertical. Thus, the SLT algorithm is applied both vertically and horizontally. Third, veins have more variable thickness compared to lane markings. It is common practice to use multiple kernels with variable thicknesses in vein segmentation. In the proposed algorithm, similar logic is applied. The SLT algorithm uses a range to calculate $Average_L$ and $Average_R$ (i.e. the number of pixels used to calculate the average). To consider both thick and thin veins, the SLT algorithm is applied twice with a low range value (12 pixels) and a high range value (25 pixels) for both vertically and horizontally (please note that these values are selected for the HRF database and when testing with the DRIVE dataset, thickness values are changed directly according to the ratio between the image width of the HRF images and the image width of the DRIVE images). Thus, the input image is filtered with the SLT algorithm four times in total: two times in the vertical direction with different range values and two times in the horizontal direction with different range values. Each feature map is then passed through image erosion and then image dilation to remove disconnected noises before applying a logical "OR" operator. Input and output feature maps can be seen in Figure 6. Subsequently, these four feature maps are combined using a logical "OR" operator. The pseudocode of the algorithm is shown in Algorithm 2.

2.4. Postprocessing using major axis length

Connected component analysis and filters like the median filter are the most commonly applied techniques to eliminate disconnected noises such as salt and pepper noise. It is already known that the veins are stripes. Thus, even if there is a discontinuity, in the extracted vein one axis needs to be much larger than the other

Algorithm 2 Multiscale Multidirectional SLT

$F \leftarrow \emptyset$
$Fh1 \leftarrow \emptyset$
$Fh2 \leftarrow \emptyset$
$Fv1 \leftarrow \emptyset$
$Fv2 \leftarrow \emptyset$

while $I_p \in ImageSize$ **do**
  if $I_p + T_h < Average_{R1}$ && $I_p + T_h < Average_{L1}$ **then**
    $Fh1_{Ip} \leftarrow 1$
  end if
  if $I_p + T_h < Average_{R2}$ && $I_p + T_h < Average_{L2}$ **then**
    $Fh2_{Ip} \leftarrow 1$
  end if
  if $I_p + T_h < Average_{Up1}$ && $I_p + T_h < Average_{Down1}$ **then**
    $Fv1_{Ip} \leftarrow 1$
  end if
  if $I_p + T_h < Average_{Up2}$ && $I_p + T_h < Average_{Down2}$ **then**
    $Fv2_{Ip} \leftarrow 1$
  end if
end while

Erode $Fh1$ **then** *Dilate* $Fh1$
Erode $Fh2$ **then** *Dilate* $Fh2$
Erode $Fv1$ **then** *Dilate* $Fv1$
Erode $Fv2$ **then** *Dilate* $Fv2$

$F = Fh1 \mid Fh2 \mid Fv1 \mid Fv2$

axis. Thus, such a connected component has much larger perimeter compared to a connected component of the same size (total number of connected pixels). This can be observed in Figure 7. In Figure 7, two examples of connected components are shown. When the properties of connected components in the figure are measured, the connected component on the left consists of 40,449 pixels and its major axis length is measured as 140 (major axis length is the distance between the two farthest pixels in a connected component). On the other hand, the connected component on the right consists of only 2028 pixels and its major axis length is measured as 156. It is a common approach to use connected component analysis to remove small sized noises by filtering based on the number of connected pixels. However, since veins have a stripe-like shape and resemble the shape shown on the right, it makes sense to use major axis length to eliminate small objects for vein segmentation. Accordingly, the major axis length of each connected component is measured and disconnected components are eliminated based on this metric. An example of an input feature map and its output feature map can be seen in Figure 8.

3. Results and discussion

To quantify the performance of the algorithm, the publicly available High-Resolution Fundus (HRF) image database [4] is used. In this database, both healthy retinas and pathological retinas with their hand-labeled ground-truths are provided. The database includes images from healthy eyes, eyes with signs of diabetic

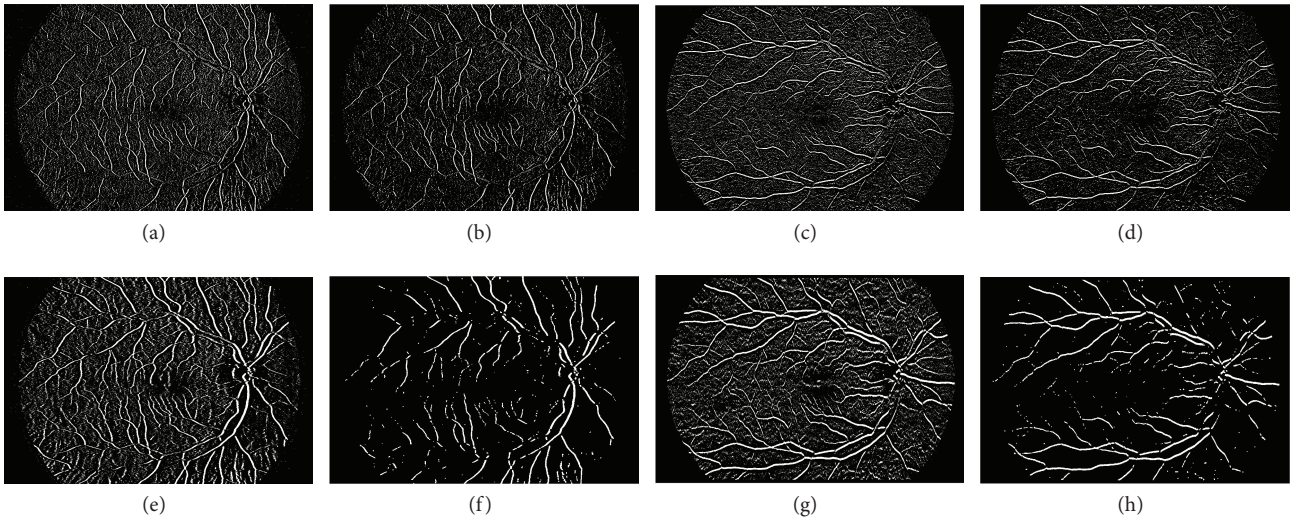

Figure 6: Combined feature maps: (a) thin vertical vein segmentation, (b) its output after morphological operations, (c) thin horizontal vein segmentation, (d) its output after morphological operations, (e) thick vertical vein segmentation, (f) its output after morphological operations, (g) thick horizontal vein segmentation, (h) its output after morphological operations.

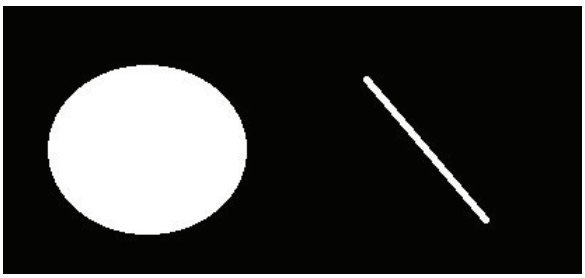

Figure 7: Example connected components, where on the left a connected component with a total number of 40,449 pixels and with a major axis length of 140 is shown. On the other hand, on the right, a connected component with a total number of 2028 pixels and with a major axis length of 156 is shown.

retinopathy, and eyes with signs of glaucoma. The dataset provides 15 images for each group. Examples of input images and their segmented outputs are provided in Figure 9. To quantify the performance of the proposed algorithm, three different metrics are used: sensitivity, specificity, and accuracy. Equations for these metrics can be found below.

$$Sensitivity\ (SE) = TP/P \tag{1}$$

$$Specificity\ (SP) = TN/(TN + FP) \tag{2}$$

$$Accuracy\ (ACC) = (TP + TN)/(TP + TN + FP + FN), \tag{3}$$

where TP stands for the total number of true positives, P stands for the total number of positives, TN stands for the total number of true negatives, FN stands for the total number of false negatives, and FP stands for the total number of false positives. It should be noted that only one metric, such as accuracy, is not

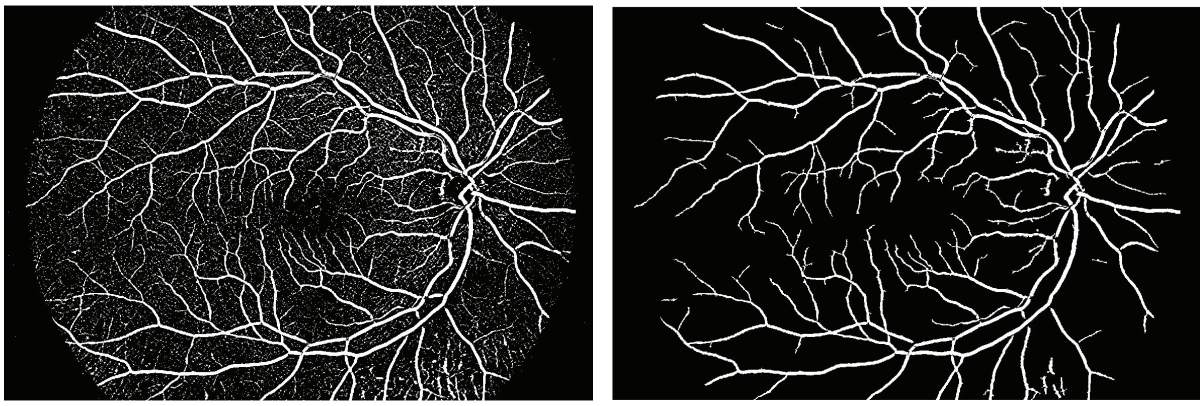

(a) (b)

Figure 8: Extracted vein feature maps beforepost processing and after postprocessing.

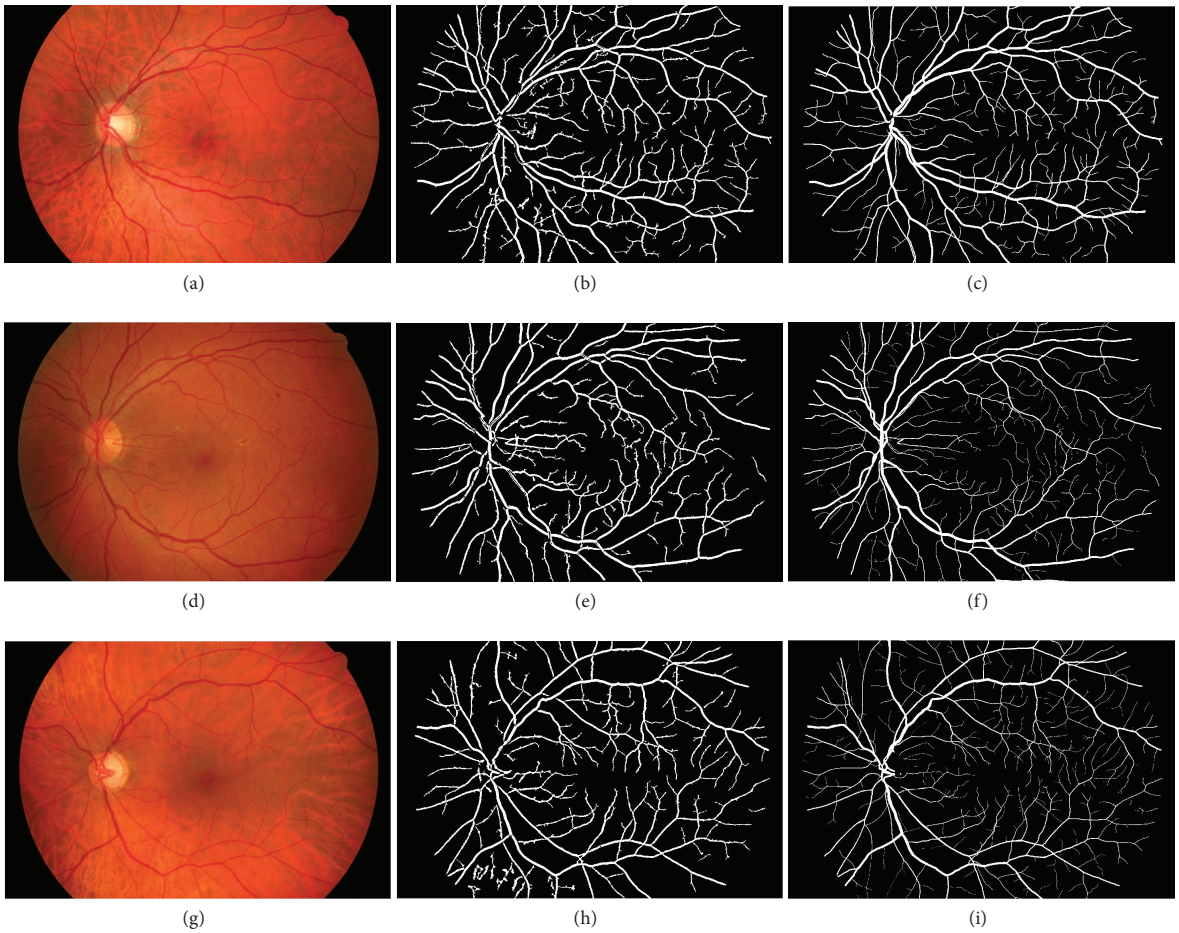

(a) (b) (c)

(d) (e) (f)

(g) (h) (i)

Figure 9: Example vein segmentation results, where in the first column input images are shown, in the second column calculated veins for the input images are shown, and in the last column manually labeled ground truth veins are shown.

enough to truly quantify the algorithm. Vein pixels are only a small portion of the total number of pixels in the image. Thus, the algorithms favoring true negatives over true positives can give higher accuracy but might not segment out vein pixels as effectively as desired. Thus, sensitivity and specificity are also important metrics. The proposed algorithm is tested for each set (three sets in total) separately and sensitivity, specificity, and accuracy are measured for each image and their calculated mean values are shown in Table 1.

In Table 1, the sensitivity, specificity, and accuracy of the proposed algorithm and the algorithms in previous studies [4, 15, 16] are shown. It is seen that the proposed algorithm outperformed the algorithm described in Odstrcilik et al. [4] in terms of sensitivity, specificity, and accuracy in all sets of images. The algorithm described in Annunziata et al. [16], while achieving good accuracy, has relatively low sensitivity compared to all other described algorithms. Compared to the algorithm described in Yu et al. [15], while in some cases their algorithm [15] performs better in terms of sensitivity and specificity, in other cases, the proposed algorithm achieves better results. On the other hand, in all cases, the proposed algorithm performs better in terms of accuracy. In Table 2 the average sensitivity, specificity, and accuracy of the algorithms are shown. In addition to the previous algorithms, in this table, results of Yang et al. [17] are also shown (no available data for this algorithm for the individual sets). From the table, it can be seen that in terms of accuracy only the algorithm in Annunziata et al. [16] performs better than the proposed algorithm. On the other hand, Annunziata et al.'s algorithm [16] has relatively low sensitivity compared to all other algorithms in the table.

Table 1: Performance evaluation on the *HRF* database.

Algorithm	Mean SE%	Mean SP%	Mean ACC%
Proposed Healthy	80.18	97.60	95.97
Odstrcilik et al.[4] Healthy	78.61	97.50	95.39
Yu et al. [15] Healthy	79.38	97.67	95.66
Annunziata et al. [16] Healthy	68.20	99.35	95.87
Proposed diabetic retinopathy	75.02	96.58	95.08
Odstrcilik et al. [4] diabetic retinopathy	74.63	96.19	94.45
Yu et al. [15] diabetic retinopathy	76.04	96.25	94.60
Annunziata et al. [16] diabetic retinopathy	69.97	97.87	95.54
Proposed glaucomatous	79.56	96.72	95.54
Odstrcilik et al. [4] glaucomatous	79.00	96.38	94.97
Yu et al. [15] glaucomatous	78.90	96.62	95.18
Annunziata et al. [16] glaucomatous	75.66	97.85	96.03

Although the HRF database [4] supplies high resolution fundus images, in the literature the DRIVE [9] database is more widely used for evaluation of retinal vessel segmentation algorithms. Thus, the proposed algorithm is also tested in the DRIVE database. The images for the DRIVE database were obtained from a diabetic retinopathy screening program in the Netherlands. The screening population consisted of subjects 25–90 years of age and 40 images are randomly selected for creating the database. Among these images, 33 do not show any sign of diabetic retinopathy and 7 show signs of mild early diabetic retinopathy. Among these 40 images, 20 are selected as the training set and the other 20 as the test set. The test set is manually labeled

twice. One set is then used as the gold standard and the other set is used for evaluating the proposed algorithm with respect to a human observer. The sensitivity, specificity, and accuracy for the second human observer are measured and the values obtained can be seen in the first row of Table 3.

It should be noted that the estimated sensitivity, specificity, and accuracy of the algorithms on the HRF database consider all the input image pixels. However, in the DRIVE database, a mask image is provided that delineates the FOV along with each input image (this was not available for the HRF database). Thus, while calculating sensitivity, specificity, and accuracy only the pixels within this mask are considered.

The sensitivity, specificity, and accuracy for the proposed algorithm on the DRIVE database can also be seen in Table 3. From Table 3, it can be noted that while the accuracy of the automated algorithms is closer to that of the human observer, the sensitivity of the human observer is by far better. Table 3 shows that in terms of accuracy the proposed algorithm outperforms those in Odstrcilik et al. [4], Al-Diri et al. [18], and Palomera-Perez et al. [19]. On the other hand, the proposed algorithm outperforms those in Odstrcilik et al. [4], Palomera-Perez et al. [19], Marín et al. [21], and Zhang et al. [20] in terms of specificity.

The proposed algorithm has an algorithmic complexity of O(N), where N is the number of pixels in the input image. The algorithm is implemented on MATLAB and the run time is measured as 2.94 s on average for the HRF database and 174 ms for the DRIVE database using $i7-8750H\ CPU$ on the HRF database. The implemented algorithm currently uses a single thread and it is also possible to improve the run time significantly by using multiple threads on multiple cores or by utilizing GPU.

Table 2: Average performance evaluation on the HRF database.

Algorithm	Mean SE%	Mean SP%	Mean ACC%
Proposed algorithm	78.25	96.97	95.53
Odstrcilik et al. [4]	77.60	96.69	94.94
Yu et al. [15]	78.10	96.85	95.15
Annunziata et al. [16]	71.28	98.36	95.81
Yang et al. [17]	79.15	96.72	95.17

Table 3: Performance evaluation on the DRIVE database.

Algorithm	Mean SE%	Mean SP%	Mean ACC%
Second human observer	78.07	97.12	94.73
Proposed algorithm	72.46	96.82	93.69
Odstrcilik et al. [4]	70.60	96.93	93.40
Marin et al. [21]	70.67	98.01	94.52
Zhang et al. [20]	71.20	97.24	93.82
Al-Diri et al. [18]	72.82	95.51	92.58
Palomera-Perez et al. [19]	64.40	96.70	92.50

4. Conclusion

In this paper, a retinal vessel segmentation algorithm has been proposed. The proposed algorithm is based on the symmetrical local threshold, which is originally designed as a feature extraction algorithm for lane detection. The lane markings and retinal vessels are similar structures in a sense that both of them represent a stripe on a digital image. In the literature, it is seen that many feature extraction algorithms for lane feature extraction and retinal vessel extraction are common such as ridge detectors, steerable filters, and matched filtering. However, SLT is designed and used only for lane detection. Furthermore, although there is no benchmarking for lane feature extractors, researchers who created the ROMA dataset tested the most common lane feature extractors and concluded that the SLT algorithm is the most robust lane feature extractor among those tested. Accordingly, in the present paper symmetrical local threshold, for the first time, is used for retinal vessel segmentation. Moreover, to be able to detect retinal vessels with a variety of thicknesses and orientations, the SLT algorithm is modified and made suitable for vessel segmentation. A lane marking has a higher intensity compared to both its left-hand side and its right-hand side. Furthermore, a retinal vessel has a darker intensity compared to both its left-hand side and its right-hand side (if the vein is vertical) or has a darker intensity compared to both its upper-hand and its lower-hand (if the vein is horizontal). Thus, instead of applying the SLT row by row horizontally as in the case of lane feature extraction, for retinal vessel segmentation, two different kernels are applied: one for horizontal vein segmentation and one for vertical segmentation. Then, considering the variation in the retinal vessels, the SLT is applied twice for each case: once for thick veins with thick SLT and once for thin veins with thin SLT. It should also be noted that applying kernels with variable thickness and orientation is a common practice for filters such as matched filters or steerable filters. By combining these outputs with a logical "OR" operator, the output gave a high response to vessels with both different thickness and orientation. While filters like the matched filter give a high response to the stripe-like pattern, it is not necessary for a structure to have a LDL pattern. On the other hand, SLT checks both sides (i.e. left and right) and ensures that both sides of the anchor pixel satisfy this property. Moreover, vessel light reflexes (a bright strip in the middle of a vessel) are not considered in this paper and can cause disruption in the middle of thick vessels. The algorithm is tested on high resolution retinal fundus images for healthy eyes, diabetic eyes, and eyes with glaucoma supplied from the HRF image database. In all categories, the proposed algorithm managed to segment retinal vessels with an accuracy of 95.53% and a sensitivity of 78.25% with a run time of 2.94 s on average using a single thread implementation. When tested with the DRIVE database, the proposed algorithm managed to segment retinal vessels with an accuracy of 93.69% and a sensitivity of 72.46% with a run time of 174 ms on average using a single thread implementation.

References

[1] Grisan E, Foracchia M, Ruggeri A. A novel method for the automatic grading of retinal vessel tortuosity. IEEE Transactions on Medical Imaging 2008; 27 (3): 310-319.

[2] Cheung CY, Zheng Y, Hsu W, Lee ML, Lau QP et al. Retinal vascular tortuosity, blood pressure, and cardiovascular risk factors. Ophthalmology 2011; 118 (5): 812-818.

[3] Youssef D, Solouma NH. Accurate detection of blood vessels improves the detection of exudates in color fundus images. Computer Methods and Programs in Biomedicine 2012; 108 (3): 1052-1061.

[4] Odstrcilik J, Kolar R, Budai A, Hornegger J, Jan J et al. Retinal vessel segmentation by improved matched filtering: evaluation on a new high-resolution fundus image database. IET Image Processing 2013; 7 (4): 373-383.

[5] Niemeijer M, Abramoff MD, Van Ginneken B. Segmentation of the optic disc, macula and vascular arch in fundus photographs. IEEE Transactions on Medical Imaging 2007; 26 (1): 116-127.

[6] Fraz M, Remagnino P, Hoppe A, Uyyanonvara B, Rudnicka et al. Blood vessel segmentation methodologies in retinal images- a survey. Computer Methods and Programs in Biomedicine 2012; 108 (1): 407-433.

[7] Gang L, Chutatape O, Krishnan SM. Detection and measurement of retinal vessels in fundus images using amplitude modified second-order gaussian filter. IEEE Transactions on Biomedical Engineering 2002; 49 (2): 168-172.

[8] Hoover A, Kouznetsova V, Goldbaum M. Locating blood vessels in retinal images by piecewise threshold probing of a matched filter response. IEEE Transactions on Medical Imaging 2000; 19 (3): 203-210.

[9] Staal J, Abràmoff MD, Niemeijer M, Viergever MA, Van Ginneken B. Ridge-based vessel segmentation in color images of the retina. IEEE Transactions on Medical Imaging 2004; 23 (4): 501-509.

[10] Al-Rawi M, Karajeh H. Genetic algorithm matched filter optimization for automated detection of blood vessels from digital retinal images. Computer Methods and Programs in Biomedicine 2007; 87 (3): 248-253.

[11] Vlachos M, Dermatas E. Multi-scale retinal vessel segmentation using line tracking. Computerized Medical Imaging and Graphics 2010; 34 (3): 213-227.

[12] Oliveira AFM, Pereira SRM, Silva CAB. Retinal vessel segmentation based on fully convolutional neural networks. Expert Systems with Applications 2018; 112: 229-242.

[13] Dasgupta A, Singh S. A fully convolutional neural network based structured prediction approach towards the retinal vessel segmentation. In: 14th IEEE International Symposium on Biomedical Imaging (ISBI); Melbourne, VIC, Australia; 2017. pp. 248-251.

[14] Zhu C, Zou B, Zhao R, Cui J, Duan X et al. Retinal vessel segmentation in colour fundus images using extreme learning machine. Computerized Medical Imaging and Graphics 2017; 55: 68-77.

[15] Yu H, Barriga S, Agurto C, Zamora G, Bauman W et al. Fast vessel segmentation in retinal images using multi-scale enhancement and second-order local entropy. Proceedings SPIE 8315, Medical Imaging 2012: Computer-Aided Diagnosis 2012; 8315: 83151B.

[16] Annunziata R, Garzelli A, Ballerini L, Mecocci A, Trucco E. Leveraging multiscale hessian-based enhancement with a novel exudate inpainting technique for retinal vessel segmentation. IEEE Journal of Biomedical and Health Informatics 2016; 20 (4): 1129-1138.

[17] Yang Y, Shao F, Fu Z, Fu R. Discriminative dictionary learning for retinal vessel segmentation using fusion of multiple features. Signal, Image and Video Processing 2019; 13: 1529-1537.

[18] Al-Diri B, Hunter A, Steel D. An active contour model for segmenting and measuring retinal vessels. IEEE Transactions on Medical Imaging 2009; 28 (9): 1488-1497.

[19] Palomera-Perez MA, Martinez-Perez ME, Benitez-Perez H, Ortega-Arjona JL. Parallel multiscale feature extraction and region growing: application in retinal blood vessel detection. IEEE Transactions on Information Technology in Biomedicine 2009; 14 (2): 500-506.

[20] Zhang B, Zhang L, Zhang L, Karray F. Retinal vessel extraction by matched filter with first-order derivative of Gaussian. Computers in Biology and Medicine 2010; 40 (4): 438-445.

[21] Marín D, Aquino A, Gegundez-Arias ME, Bravo JM. A new supervised method for blood vessel segmentation in retinal images by using gray-level and moment invariants-based features. IEEE Transactions on Medical Imaging 2010; 30 (1): 146-158.

[22] Schreiber D, Alefs B, Clabian M. Single camera lane detection and tracking. In: IEEE Conference on Intelligent Transportation Systems; Vienna, Austria; 2005. pp. 302-307.

[23] Wang Y, Lee SC. A fast method for automated detection of blood vessels in retinal images. In: IEEE Conference on Signals, Systems & Computers; Pacific Grove, CA, USA; 1997. pp. 1700-1704.

[24] Broggi A, Cappalunga A, Caraffi C, Cattani S, Ghidoni S et al. Terramax vision at the urban challenge 2007. IEEE Transactions on Intelligent Transportation Systems 2010; 11 (1): 194-205.

[25] McCall JC, Trivedi MM. An integrated, robust approach to lane marking detection and lane tracking. In: IEEE Conference on Intelligent Vehicles; Parma, Italy; 2004. pp. 533-537.

[26] McCall JC, Trivedi MM. Video-based lane estimation and tracking for driver assistance: survey, system, and evaluation. IEEE Transactions on Intelligent Transportation Systems 2006; 7 (1): 20-37.

[27] López A, Serrat J, Canero C, Lumbreras F, Graf T. Robust lane markings detection and road geometry computation. International Journal of Automotive Technology 2010; 11 (3): 395-407.

[28] Veit T, Tarel JP, Nicolle P, Charbonnier P. Evaluation of road marking feature extraction. In: IEEE Conference on Intelligent Transportation Systems; Beijing, China; 2008. pp. 174-181

[29] Ozgunalp U, Fan R, Ai X, Dahnoun N. Multiple lane detection algorithm based on novel dense vanishing point estimation. IEEE Transactions on Intelligent Transportation Systems 2017; 18 (3): 621-632.

[30] Dong S, Peng C. A lane detection method based on track management approach. In: IEEE Conference on Multisensor Fusion and Information Integration for Intelligent Systems (MFI); Beijing, China; 2014. pp. 1-6.

[31] Freeman WT, Adelson EH. The design and use of steerable filters. IEEE Transactions on Pattern Analysis & Machine Intelligence 1991; 9: 891-906.

[32] Ozgunalp U, Dahnoun N. Robust lane detection & tracking based on novel feature extraction and lane categorization. In: IEEE Conference on Acoustics, Speech and Signal Processing (ICASSP); Florence, Italy; 2014. pp. 8129-8133.